water

MDPI

Article

Fly Ash as a Catalyst for the Heterogenous Fenton Process in a Hybrid Oxidation Membrane Reactor: Optimization of Wastewater Treatment in the Winery Industry

Fadhila Malahayati Kamal [1], Sucipta Laksono [1,*], Sandyanto Adityosulindro [1], Lucas Landwehrkamp [2] and Stefan Panglisch [2]

[1] Environmental Engineering Study Program, Department of Civil Engineering, Faculty of Engineering, Universitas Indonesia, Depok 16424, Indonesia; fadhila.malahayati21@gmail.com (F.M.K.); rm.sandy.ui@gmail.com (S.A.)
[2] Mechanical Process Engineering and Water Technology, University of Duisburg-Essen, 47057 Duisburg, Germany; lucas.landwehrkamp@uni-due.de (L.L.); stefan.panglisch@uni-due.de (S.P.)
* Correspondence: suciptalaksono@gmail.com

Abstract

The growing global population has increased energy and food demand, leading to a higher production of waste streams such as fly ash from the energy sector and wastewater from food and beverage industries. Without proper treatment, these wastes pose significant environmental concerns. One promising strategy is to repurpose industrial byproducts for wastewater treatment. Winery wastewater, for instance, contains acidic organic compounds and alcohol that are difficult to remove using conventional methods, while large amounts of fly ash remain underutilized. This study, therefore, examines a hybrid system that combines fly ash-assisted Fenton oxidation with membrane filtration for winery wastewater treatment. The process involved sequential Fenton pre-treatment followed by lab-scale nanofiltration using a 1 kg/mol ceramic membrane (13.1 cm^2). A Design of Experiments approach was applied to evaluate system performance under varying H_2O_2 dosages (10–30 mL/L), fly ash loadings (1–3 g/L), and membrane fluxes (40–80 LMH). Filtration was performed through multiple constant-flux cycles, with energy requirements ranging from 400 to 800 kWh/m^3 for the flux variations calculated from the lab-scale pump operating at a constant power supply. The hybrid method showed strong performance, achieving 70% TOC removal and 90% reduction of color and iron. However, considerable membrane fouling was observed, likely due to increased retention and deposition of organic matter, iron, and fly ash during filtration.

Keywords: fly ash; heterogeneous Fenton; membrane filtration; membrane fouling; winery wastewater

Academic Editor: Jesus Gonzalez-Lopez

Received: 21 May 2026
Revised: 25 June 2026
Accepted: 27 June 2026
Published: 6 July 2026

1. Introduction

The global alcoholic beverage market is influenced by cultural preferences and contributes to worldwide commercialization and consumer behavior [1]. Wine production in particular is a multi-step process that generates a significant volume of wastewater [2]. The volume of wastewater varies with production scale, ranging from 0.2 to 4 L per liter of wine [3]. The characteristics of wine wastewater result in significant challenges for wastewater treatment plants due to its acidic nature (pH 4–5), high organic content (COD with 340 mg/L to 360,000 mg/L, and TOC with 7363 mg/L), and intense color (up to

6500 Pt-Co) [3,4]. In detail, wine production wastewater consists of various organic compounds, including sugars, ethanol, organic acids, aldehydes, and high molecular weight compounds such as polyphenols, tannins, and lignin [5]. Additionally, detergents from cleaning processes contribute to the complex organic composition of winery wastewater [4].

Given the high organic content, winery wastewater requires effective degradation processes; it has historically been treated using conventional biological treatments such as aerobic and anaerobic systems. Although these methods are relatively cost-effective [6], they present several limitations. Anaerobic treatment often achieves incomplete organic removal (limited to less than 90%) [7] and typically requires another form of secondary treatment [6], while its operation demands skilled control to maintain stable sludge blanket conditions. Seasonal fluctuations between vintage and non-vintage periods in the winery industry further complicate process stability, as microbial populations become difficult to sustain year-round. Moreover, aerobic systems designed to handle peak harvest loads tend to be oversized during off-season periods, leading to operational inefficiencies [3,6] and also the treatment efficiency was lower than that achieved by the anaerobic process [8]. The high-strength nature of winery wastewater can also promote excessive biomass growth, increase aeration requirements, and generate large volumes of sludge that pose additional handling and disposal challenges [9,10]. Therefore, these limitations have driven increasing interest in advanced and hybrid treatment technologies capable of more effectively addressing the high organic load and complex composition of winery wastewater.

One alternative process to treat complex winery wastewater employs a heterogeneous Fenton process, with recent studies revealing significant efficiency of up to 90% in organic removal [11–13]. The higher efficiency is attributed to the production of reactive oxygen species (°OH and °OOH) generated by H_2O_2 as an oxidizing agent and Fe^{2+} or Fe^{3+} as catalysts under acidic conditions [14,15]. The optimal pH range for heterogeneous Fenton reactions ranges between pH 3 and pH 6 [16], thus revealing its versatility and adaptability in treating winery wastewater. Heterogeneous Fenton processes can also utilize solid catalysts as a source of Fe [17], creating opportunities for a variety of materials to be used as catalysts. However, the application of solid catalysts introduces concerns about iron leaching [18]. This phenomenon involves iron species on the catalyst surface dissolving and escaping into the surrounding liquid as dissolved iron [19].

Coal fly ash (CFA), a waste residue abundantly generated by thermal power plants worldwide, poses a significant environmental issue due to the water and soil contamination risks associated with improper disposal [20]. CFA consists of metal-rich oxides such as SiO_2, Al_2O_3, or Fe_2O_3 [21], indicating a potential application as a Fenton catalyst, especially due to its high iron content. The potential of CFA for the removal of various pollutants, such as organic matter from leachate, dye, polyacrylamide, as well as wastewater-related organic matter through a heterogeneous Fenton reaction has already been demonstrated [20–25]. In a study conducted by (Zhao, Yuxuan et al.), coal fly ash-based catalysts used in heterogeneous Fenton processes exhibited excellent catalytic activity and stability [26]. Similarly, another study reported that fly ash demonstrated satisfactory reusability after several consecutive operating cycles. These findings suggest that fly ash is a promising and cost-effective catalyst for the degradation of organic dyes in aqueous solutions through heterogeneous Fenton processes [27].

Besides heterogeneous Fenton processes, membrane technology has gained significant attention in industrial wastewater treatment, especially in cases where high effluent qualities are necessary [28]. For winery wastewater treatment, nanofiltration and reverse osmosis membranes are commonly employed due to their high efficiency in pollutant removal [4]. The combination of membrane processes with other water treatment technologies results in the so-called “hybrid process” [29].

The coupling of membrane filtration and advanced oxidation processes (AOPs), including Fenton-based reactions, has emerged as a growing area of research in water treatment technology. This combined approach has attracted significant attention because of its potential to permanently resolve or mitigate membrane fouling issues and address the challenge of managing concentrate waste generated during membrane separation [30]. The distinct advantages of this coupled process are largely attributed to the high organic content present in winery wastewater. When applied as a pre-treatment stage, the Fenton process can effectively degrade organic compounds in the membrane feed stream. It is primarily intended to reduce membrane fouling through the oxidation of natural organic matter (NOM), particularly humic acids [31]. Research related to Fenton–membrane configurations for the treatment of industrial wastewater, particularly in the textile industry, has demonstrated its ability for the removal of organic substances, resulting in an over 75% reduction of dissolved organic carbon [32]. In a recent study conducted by (He, Yulun et al.) [33], a Fenton catalytic membrane was employed for the treatment of micropollutants. The results were highly satisfactory, achieving up to 97.4% removal of bisphenol-A (BPA). The experiments demonstrated a stable performance of the hybrid process across a wide variety of pH levels, indicating its high potential for future drinking water treatment applications.

Based on the previously mentioned advantages of this hybrid system, the integrated process can provide higher purification efficiency, improved membrane flux with reduced fouling, and the added benefit of enabling separation of the solid catalyst from the treated water. The superiority of hybrid processes represents a significant advancement that encourages further research on the recovery of industrial wastewater for specific reuse purposes [32,34]. Water recovery is often not feasible using conventional treatment methods; therefore, advanced technologies such as hybrid processes are required [31,35]. In several development studies, the oxidation of organic compounds has shown significant improvement through the integration of additional processes into hybrid Fenton–membrane systems. Furthermore, such modifications may provide solutions to other challenges, particularly those related to membrane durability against cavitation. In ultrasound-assisted studies, experiments were conducted by combining these processes to achieve higher organic pollutant removal efficiencies while simultaneously reducing the risk of membrane cavitation [35]. These studies highlight the potential for further enhancement of hybrid Fenton–membrane systems.

A comprehensive evaluation of the hybrid process's effectiveness necessitates the variation of a wide range of operational parameters or variables from each component process. In this study, Design of Experiment (DOE) methodology was employed for the analysis of the individual and combined influence of selected operational parameters on process performance with a minimum number of experiments. In this study, the removal of total organic carbon and color, as well as the iron concentration in the permeate of the membrane process, were used as quality parameters.

2. Materials and Methods

2.1. Characterization of Synthetic Winery Wastewater

The experiments were carried out employing synthetic winery wastewater in order to imitate winery wastewater characteristics. Synthetic wastewater was prepared by diluting commercial red wine with domestic greywater at a ratio of 1:100. This ratio was selected to better represent realistic operating conditions, as winery wastewater is characterized by a very high organic load (with COD concentrations ranging from 340 mg/L to 360,000 mg/L) [3,4]. Furthermore, the selected ratio is consistent with the primary objective of this study, which focuses on the treatment of high-strength organic wastewater. A study comparing direct membrane filtration performance using synthetic wastewater

and real wastewater with high organic content revealed that it can serve as a suitable surrogate for DMF investigations. The use of synthetic wastewater helps minimize one of the major sources of variability in current DMF studies, thereby facilitating more consistent experimental conditions and supporting the accelerated development of DMF technology [36]. The greywater was sourced from a wastewater treatment plant in South Jakarta, the characteristics of which are detailed in Appendix A.1. The characteristics of the winery wastewater are presented in Table 1.

Table 1. Properties of synthetic winery wastewater.

Parameter	Unit	Value
pH	-	3
COD	mg/L	3850
TOC	mg/L	1178
Total Iron	mg/L	2
Color	Pt-Co	120

2.2. Modification of Fly Ash Iron Oxide (FA-Fe_3O_4)

Nanoparticles of Fe_3O_4 were synthesized on CFA obtained from the thermal power plant in South Sulawesi, Indonesia, using inverse co-precipitation to create FA-Fe_3O_4 [22]. A 60 mL solution of 10% ammonium hydroxide (NH_4OH) was mixed with 2 g of CFA. Moreover, an iron precursor solution, prepared by dissolving $FeSO_4 \cdot 7H_2O$ (1 M) (99.5%, analytical grade, Merck, Darmstadt, Germany) and $FeCl_3$ (2 M) (99%, analytical grade, Merck, Darmstadt, Germany) in 30 mL of deionized water, was slowly added to the base solution under constant agitation at 450 rpm and a temperature of 60 °C. Furthermore, the mixture was stirred for 90 min. Thereafter, the mixture was filtered, rinsed, and dried in the oven overnight at 105 °C. The augmented CFA with iron oxide was further characterized. The crystalline phases present in the catalysts were identified using X-ray diffraction (XRD). The diffraction patterns of FA-Fe_3O_4 were recorded in the 10° to 90° at 2θ. Scanning electron microscopy (SEM) equipped with energy-dispersive X-ray spectroscopy (EDS) (Apreo SEM, Thermo Fisher Scientific, Waltham, MA, USA). was used to investigate the surface morphology and elemental composition of FA-Fe_3O_4. In parallel, the size distribution of FA-Fe_3O_4 was characterized through Particle Size Analysis.

2.3. Hybrid Fenton–Membrane Experiments

A lab-scale hybrid Fenton membrane experiment was conducted, initially employing 500 mL of synthetic winery wastewater. The wastewater underwent the Fenton oxidation process with the addition of various concentrations of H_2O_2 (10–30 mL/L) (30%, analytical grade, Merck, Darmstadt, Germany) and FA-Fe_3O_4 (1000–3000 mg/L) in a 1000 mL beaker glass. Based on the characteristics of the synthetic winery wastewater presented in Table 1, the varied H_2O_2 dosages correspond to mass-based $gH_2O_2/gTOC$ ratios of 2.8:1, 5.7:1, and 8.5:1, respectively. The solution was then stirred at 350 rpm at room temperature for 60 min to maintain homogeneous conditions during filtration.

Thereafter, synthetic wine wastewater was filtered through the membrane holder employing a peristaltic pump (Longer BT 100-1F, Longer Precision Pump Co., Ltd., Baoding, Hebei, China). The pump was working with a power supply of 90 V–260 V/40 W) (Figure 1). In the membrane filtration process, a flat-sheet ceramic membrane made of ZrO_2–TiO_2 was used. The membrane had a diameter of 47 mm, a thickness of 2.5 mm, and an effective surface area of 13.1 cm^2. It was manufactured by TAMI Industries and had a molecular weight cut-off (MWCO) of 1 kg/mol (≈2 nm). The filtration system was operated under a dead-end and constant flux mode by adjusting the peristaltic pump to the required

flow rate. Due to the dead-end mode, the entire volume of the introduced feed was directed perpendicularly through the membrane pores; a feed circulation loop was absent, making feed circulation metrics not applicable to this experimental setup. Furthermore, this dead-end design operated without a continuous concentrate bleed-off stream, meaning that the volume of the generated permeate mathematically matched the processed feed volume. This configuration established an effective, constant water recovery percentage of approximately 100% for each cycle. Under these strict constant-flux boundary conditions, the progressive hydraulic resistance was directly evaluated by monitoring changes in the operational transmembrane pressure (TMP) rather than a decline in fluid recovery.

For each experiment, multiple filtrations of 4 cycles were performed at room temperature with a filtration time of 15 min per cycle in order to assess the immediate effect of the factors on the filtration process. The volume of permeate water was measured with a digital analytical balance, and the pressure difference was also measured by a pressure gauge and recorded at each minute of the filtration time. Thereafter, in each cycle, the membrane went through a mechanical backwash process for 60 s using pure water. The backwash process was performed by reversing the flow of ultrapure water through the membrane to reduce the membrane fouling [32]. The permeate from all four cycles was then collected and combined for TOC, color, and iron concentration analysis.

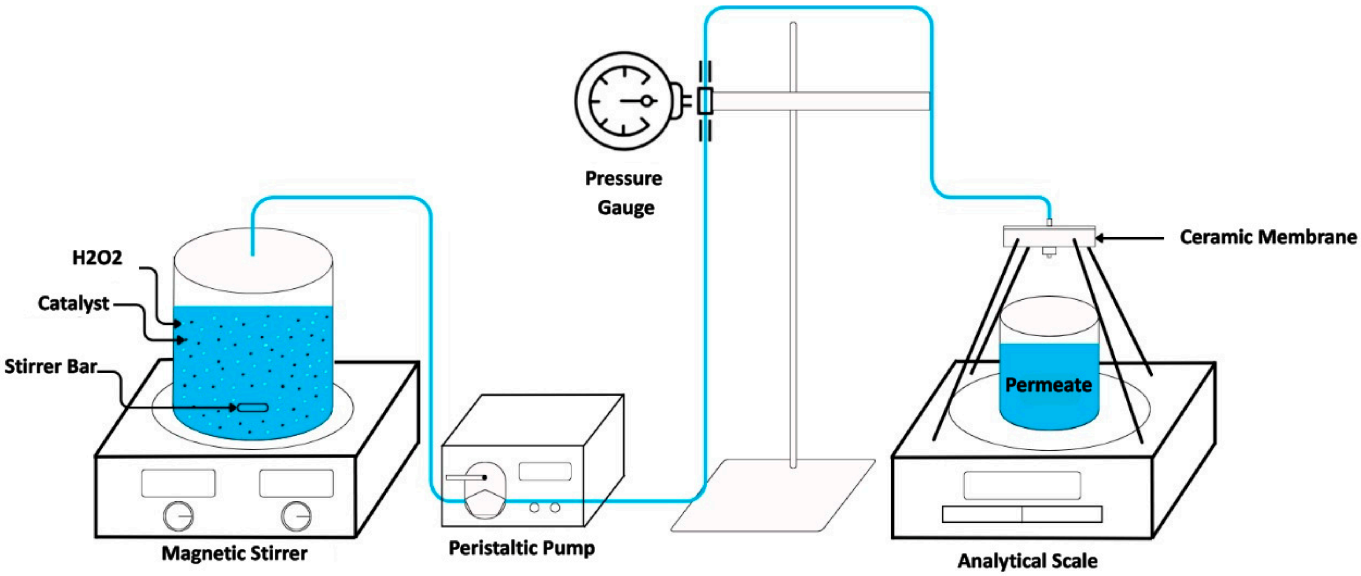

Figure 1. Hybrid Fenton-membrane filtration experiment setup.

After multiple filtration processes were performed, the membrane was cleaned using cleaning agents of NaOCl 5% (v/v) (technical grade, OneMed, Sidoarjo, Indonesia), followed by backwashing and filtration using ultrapure water. The same ceramic membrane was used for all of the experiments. The membrane was cleaned between experiments using a Cleaning in Place (CIP) procedure in order to remove fouling caused by inorganic and organic matter [37]. NaOCl 5% mg/L was used in the cleaning process in order to remove organic foulants, while citric acid (6%) was used to remove inorganic foulants from the previous filtration process of synthetic winery wastewater [37]. Details of the membrane filtration procedure are described in Figure 2.

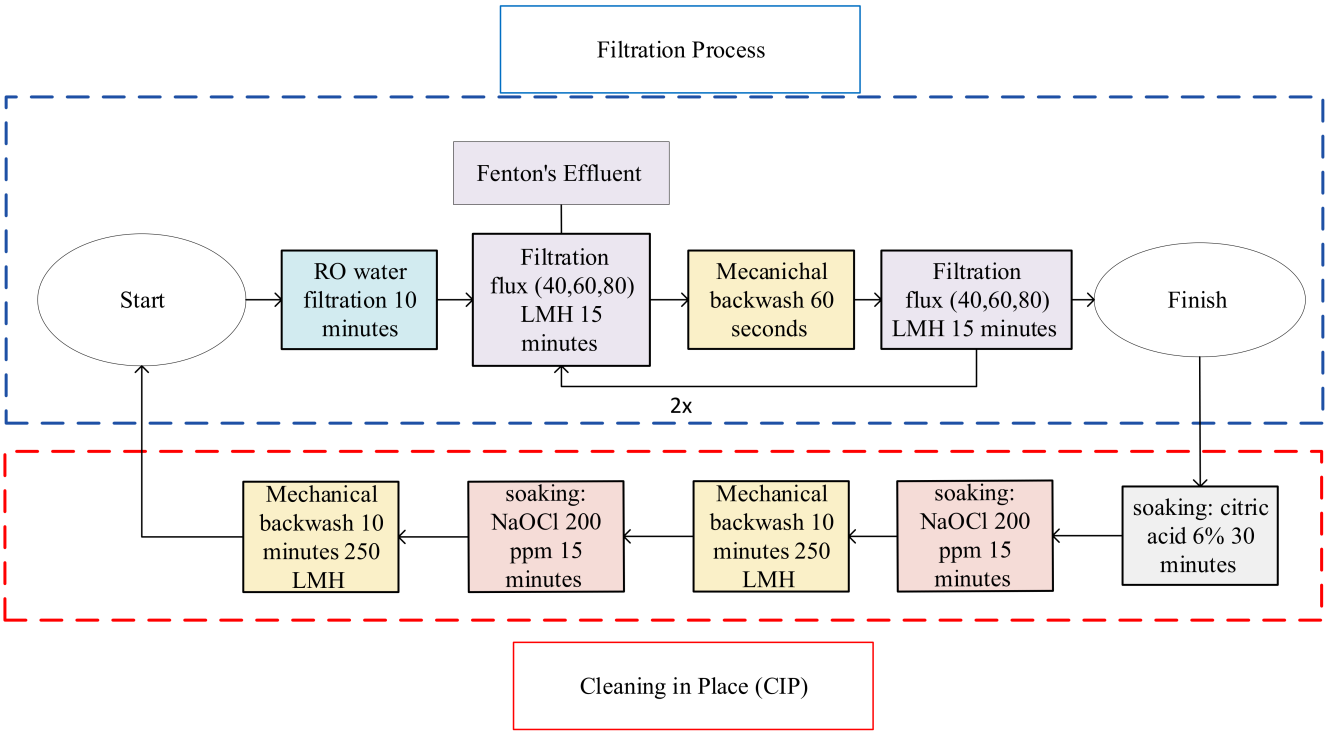

Figure 2. Filtration process and CIP flow chart.

2.4. Performance Assessment

2.4.1. Hybrid Reactor Efficiency

All of the samples were collected after the Fenton and filtration process to analyze the target parameters, consisting of TOC, color, and iron concentration. The TOC concentration was measured with a TOC analyzer (TOC-L, Shimadzu Corporation, Kyoto, Japan) according to the Standard Method 5310 (Total Organic Carbon). Thereafter, the color parameter was measured according to the standard method 2120. The removal rates of TOC and color were calculated through Equation (1).

$$\eta\% = \frac{C_0 - C_t}{C_0} \times 100\% \quad (1)$$

where C_0 and C_t are the initial concentration and residual concentration of TOC (mg/L) or color (Pt-Co) and η is the removal rate. Moreover, the total Fe (mg/L) was measured through the FerroVer method according to the HACH Method 8008.

2.4.2. Membrane Performance

Membrane filtration performance was assessed through the fouling behavior of each experiment, investigated by measuring the membrane permeability decay of each cycle. Membrane permeability (W, L/m^2.hour/bar) was calculated by Equation (2).

$$W = \frac{J}{\Delta P} \quad (2)$$

$$J = \frac{Q}{Am} \quad (3)$$

where J is water flux (L/m^2.hour) obtained from the collection of the filtered volume rate (Q, L/h) divided by the active surface area (Am, m^2). Moreover, ΔP is the transmembrane pressure (bar). The membrane performance decay during the filtration was monitored by plotting the permeability (W) vs specific filtered volume (Vsp). The specific filtered volume

(Vsp) was calculated as the product of permeate flux (J) and the filtration time (t). This parameter represents the cumulative volume of permeate produced per unit membrane area during the filtration process and was used to evaluate membrane performance and fouling behavior over time (see Equation (4)).

$$\mathrm{Vsp} = J \times t \tag{4}$$

2.5. Design of Experiment (DoE)

A two-stage factorial design introduced by Kleppmann was employed to optimize the experimental design and systematically adjust the parameters within a certain range of values [38]. The variables investigated in this study consist of H_2O_2 (10–30 mL/mL), the catalyst (1000–3000 mg/L), and flux (40–80 LMH). To model the second-order effects, a central composite design (CCD) was selected. This was done because a full factorial design with three stages requires a higher number of experiments. Consequently, a 2^3 full factorial experimental design, along with a center point and an additional $2 \times 3 = 6$ star points were created. A center point is an additional measurement location at the center of the test area, and star points are situated at the edges, slightly outside the typical range for a particular parameter. Subsequently, an orthogonal experimental design was generated with respect to all terms in the model through Equation (5).

$$\propto^2 = \frac{1}{2}\left(\sqrt{\mathrm{N} \times \mathrm{N_s}} - \mathrm{N_s}\right) \tag{5}$$

where $\propto$ is the distance between central points and star points, N_s is the number of experiments for the full factorial design without a center point (here $N_s = 2^3 = 8$), and N is the total number of experiments for the CCD design. Consequently, the total number of experiments (N) in this study is 16, consisting of 8 full factorial experiments, 6 experiments of star points, and 2 center points. The $\propto$ coded value of the individual factors and their corresponding non-coded value are summarized in Table 2, and the 16-design matrix of the overall experiments is shown in Table 3. Thereafter, all the samples from the 16 experiments were tested for TOC, color, and iron concentration, and the results were further analyzed using the statistical analysis tools in JMP® version 18.

Table 2. Experimental range and levels.

Factors	Unit	$\propto = -1.41$	−1	0	1	$\propto = 1.41$
H_2O_2	mL/L	5.86	10	20	30	34.15
Catalyst	mg/L	590	1000	2000	3000	3420
Flux	LMH	31.72	40	60	80	88.29

Table 3. Design matrix and permeate water quality, as well as efficiency.

	No	H_2O_2 (mL/L)	Catalyst (mg/L)	Flux (LMH)	Color (Pt-Co)			Total Organic Carbon (mg/L)			Permeate Iron Concentration (mg/L)
					Feed	Permeat	Removal (%)	Feed	Permeate	Removal (%)	
Factorial points	1	10	1000	40	117	29	75	1178	705	40	1
	2	30	1000	40		17	85		586	50	0
	3	10	3000	40		12	90		593	50	1
	4	30	3000	40		12	90		586	50	2
	5	10	1000	80		23	80		504	57	12
	6	30	1000	80		29	75		375	68	1
	7	10	3000	80		15	87		360	69	5
	8	30	3000	80		13	89		404	66	2
Axial points	9	5.86	2000	60		19	84		404	66	2
	10	34.15	2000	60		18	85		381	68	4
	11	20	590	60		21	82		481	59	3
	12	20	3420	60		16	86		491	58	5
	13	20	2000	31.72		19	84		353	70	6
	14	20	2000	88.29		21	82		464	61	2
Center points	15	20	2000	60		18	85		488	59	3
	16	20	2000	60		13	89		492	58	4

3. Results and Discussions

3.1. Modified Fly Ash Iron Oxide (FA-Fe_3O_4) Characterization

Characterization was performed through X-ray Diffraction (XRD) analysis to identify the phase fraction in the FA-Fe_3O_4 catalyst. The XRD diffraction pattern showed peaks at various angles. These angular peaks had high intensities at 30.97°, 35.26°, 41.60°, 50.72°, 67.62°, and 74.57°, as shown in Figure 3a. This indicates the presence of Magnetite (Fe_3O_4), Hematite (Fe_2O_3), Aluminum Silicon Oxide (Al_2SiO_5), and Silicone Dioxide (SiO_2). The detection of Magnetite confirms the successful incorporation of Fe_3O_4 into the fly ash, enhancing its potential catalytic properties. Moreover, the presence of other compounds contributes to the structural matrix of the fly ash and explains the typical composition of fly ash [39].

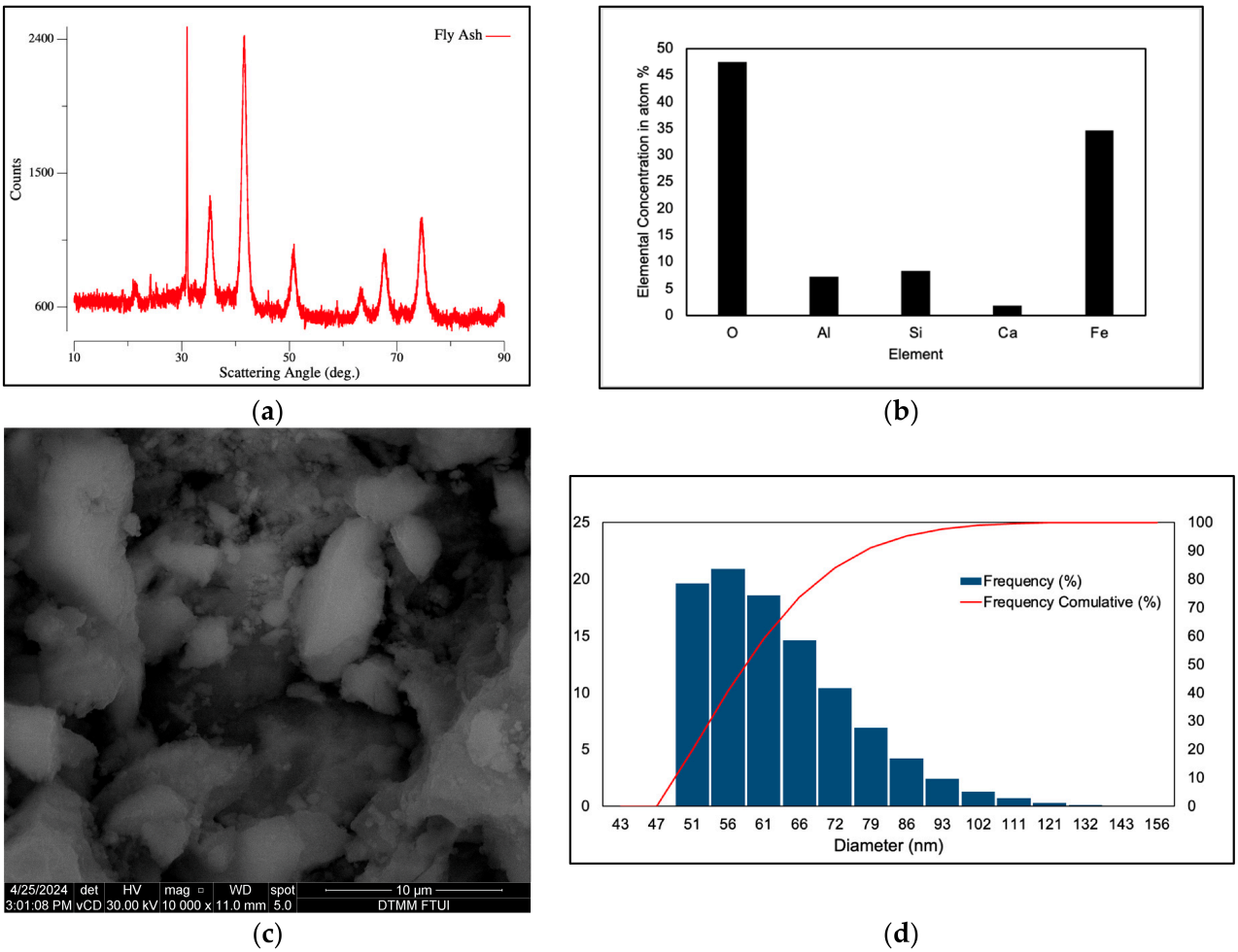

Figure 3. Characterization of modified FA-Fe_3O_4: (**a**) XRD Pattern; (**b**) Elemental Concentration; (**c**) SEM Image; and (**d**) Particle Size Distribution.

Further Characterization was also conducted to identify the surface morphology of FA-Fe_3O_4 using Scanning Electron Microscopy (SEM) equipped with Energy Dispersive Spectroscopy (EDS). As shown in Figure 3c, FA-Fe_3O_4 has an eccentric shape with an irregular morphology at a magnification of 10,000×. Moreover, the elemental composition (Figure 3b) shows that FA-Fe_3O_4 is dominated by oxygen (O) and iron (Fe) with atom concentrations of 47.5% and 34.59%, respectively. The abundance of oxygen reflects its role in both the fly ash matrix and the iron oxide. Silicon (Si), aluminum (Al), and calcium (Ca) appear in relatively low amounts with atom concentrations of 8.32%, 7.31%, and 1.76%, respectively. Moreover, the data suggest that the augmented fly ash could be effective in

applications for heterogeneous Fenton reactions. This is supported by the preliminary experiments of this study that revealed the limited capacity for color removal when FA used independently (see Appendix A.5). The augmentation of Fe_3O_4 onto the FA surface was essential to boost catalytic performance. This concluded that the high iron content and reactive surface area were found to be crucial for generating hydroxyl radicals [17].

The particle size distribution analysis of FA-Fe_3O_4 (Figure 3d) revealed a broad range of sizes from 51 to 132 nm, with a dominant population concentrated between 51 and 66 nm. The average particle size was determined to be 64.2 nm, classifying it as an ultrafine fly ash catalyst that offers distinct advantages for heterogeneous Fenton reactions [40]. These nanoscale dimensions enhance reactivity by significantly increasing the available surface area for oxidative reactions at the interface between the solid catalyst and the liquid H_2O_2 phase to generate hydroxyl radicals [17,41]. This high performance is fundamentally rooted in the synergistic interaction between the Fe_3O_4 and the coal fly ash (CFA) matrix, where the CFA acts as critical support that prevents the magnetic self-aggregation of the nanoparticles. Furthermore, structural stability is reinforced by the 'anchoring' of these nano-sites onto larger CFA granules, as evidenced by the high Polydispersity Index (1.024) and the detection of micro-scale peaks at 2073.5 nm, as shown in the PSA detailed results shown in Appendix A.6. This correlation with the granular morphology observed in SEM is essential for operational stability; the micro-scale support ensures efficient retention by the ceramic membrane, maintaining catalytic activity and allowing membrane permeability to be recovered across multiple filtration cycles without the loss of the active nanophase.

3.2. Hybrid Fenton–Membrane Removal of Synthetic Winery Wastewater

The results showed that the combination of the factors resulted in pollutant degradation with removal efficiencies exceeding 40% in all experiments for TOC and color. The removal of TOC and color is attributed to the mechanism of Fenton and membrane filtration to remove pollutants. In the heterogeneous Fenton oxidation process, the interaction between Fe^{2+} and Fe^{3+} present in FA-Fe_3O_4 and H_2O_2 leads to the formation of reactive oxygen species [42]. The reactive species are primarily responsible for the degradation of TOC and color in synthetic winery wastewater. According to the XRD characterization results (Figure 3a), magnetite is the dominant phase in FA-Fe_3O_4, ensuring optimal interactions between Fe^{2+} and Fe^{3+} with H_2O_2. Consequently, both the catalyst and H_2O_2 individually and synergistically contribute significantly to TOC and color removal. This was shown in experiments where the H_2O_2 and catalyst dosage were operating at the same flux (experiments 1–4 with flux 40 LMH and 5–8 with flux 80 LMH, see Table 3), resulting in different removal efficiencies. This is supported by a preliminary study showing that the presence of H_2O_2 in the Fenton process using FA-Fe_3O_4 as a catalyst increases color removal by 35% compared to adsorption alone (Appendix A.2). Similarly, another study concluded that introducing H_2O_2 in the Fenton process post-adsorption increases color removal by 30% [43]. Consistent with these findings, research demonstrated that the interaction between FA-Fe_3O_4 and H_2O_2 effectively removes up to 70% of COD from wastewater [22].

In addition to the contribution of the heterogeneous Fenton oxidation process, the operational parameter of filtration flux was also identified as a parameter that provides a high contribution to TOC removal. Referring to the removal results in Table 3, experiments with fluxes of 80 LMH and 88 LMH (experiments 5–8 and 14) resulted in the highest TOC removal with a range of 65% to 70% compared to lower flux variations. This is triggered by the need to maintain constant flux operational conditions at 80 LMH, which requires a comparably higher pressure related to fluxes of 39 to 60 LMH. Operating the filtration system at an elevated pressure and flow rates is proven to accelerate the membrane

fouling [44]. Furthermore, the resulting fouling layer, composed of organic pollutants and FA-Fe_3O_4 solid catalysts, acts as an additional membrane, potentially enhancing TOC removal. At higher pressures, denser cake layers with smaller pore sizes can be formed [45]. A previous study demonstrated that elevating the operational pressure of membrane filtration from 1 to 3 bar yielded a threefold enhancement in COD removal [46].

The observed TOC removal of approximately 70% can be attributed to the combined effects of oxidative degradation and membrane separation in the hybrid treatment system. In the Fenton process, TOC reduction primarily occurs through the oxidation of organic compounds by hydroxyl radicals (•OH) generated from the reaction between ferrous ions and hydrogen peroxide [47]. This removal is further enhanced during the membrane filtration step via size exclusion and electrostatic interactions between organic solutes and the membrane surface.

Considering the high organic content and complex composition of winery wastewater, this level of performance can be regarded as satisfactory. Comparable TOC removals of 68.9% have been reported by Jing Xu et al. (2017) under similar operating conditions using a Fenton process coupled with nanofiltration for high-TOC wastewater [15]. Furthermore, a higher level of TOC removal was reported by Handan Atalay Eroğlu and Akbal (2025) [48]. In their study, the initial TOC concentration was considerably lower (18–31 mg/L), and reverse osmosis (RO) was used as the final treatment step. RO membranes provide tighter separation, capable of rejecting even low-molecular-weight organic compounds and dissolved ions, which naturally leads to higher overall TOC removal. Additionally, their system operated at a higher pressure (0.4 MPa) compared to 0.2 MPa in the present study, providing a greater driving force for solute rejection [48]. Therefore, the performance observed in this study demonstrates a competitive and practically relevant level of organic matter removal while operating under relatively moderate conditions.

The iron concentration in the permeate after the filtration process from 16 experiments exhibited various concentrations ranging from 0 to 12 mg/L (Table 3). Despite an initial iron concentration of 2 mg/L (Table 1), the iron concentration on the permeate side tended to be unchanged or even increased. Out of the 16 experiments, a decrease in iron concentration only occurred in several experiments (i.e., experiments 1, 2, 3, and 6). This phenomenon was attributed to iron leaching from the FA-Fe_3O_4 catalyst during the heterogeneous Fenton process, where the iron species from FA-Fe_3O_4 turned into dissolved iron [19]. The phenomenon of iron leaching observed in this study is likely a result of the complex interaction between the acidic wastewater matrix and the catalyst surface. The dissolution of iron species occurs when the FA-Fe_3O_4 active sites undergo reductive dissolution during the Fenton cycle, especially at the interface where H_2O_2 decomposes. However, the stability of the FA-Fe_3O_4 is supported by the CFA matrix, which acts as a protective support. To evaluate catalyst integrity, a mass balance estimation based on the SEM-EDS data (Fe = 35%) indicates that this maximum dissolved fraction accounts for merely 1.14% to 3.43% of the initial structural iron present across the catalyst dosage range (1000–3000 mg/L), suggesting acceptable chemical anchoring and the mechanical robustness of the FA-Fe_3O_4 composite under the acidic Fenton conditions. However, the iron leaching phenomenon was not observed to be linear across the 16 experiments. For instance, higher iron leaching was observed at a lower catalyst dosage (experiment 5:1000 mg/L, 12 mg/L iron) compared to a higher dosage (experiment 7:3000 mg/L, 5 mg/L iron), and this non-linear trend is explained by proton-promoted dissolution under acidic conditions. At lower catalyst loading, fewer particles are present in the solution, so each particle receives a higher concentration of H^+ ions, leading to more aggressive proton-promoted iron dissolution; additionally, catalyst particles are more highly dispersed at a low dosage, creating a larger surface–acid interface per particle that allows acid and H_2O_2 to attack individual active iron

sites more aggressively; with fewer particles competing for available protons, each catalyst particle has unrestricted access to the full pool of H^+ ions, resulting in faster dissolution rates and higher iron yields [49].

Furthermore, the PSA results showing a stable peak at 2073.5 nm confirm that the bulk of the catalyst remains in a micro-scale hybrid form, which is effectively retained by the ceramic membrane. Furthermore, the nanofiltration membrane size with a molecular weight cutoff (MWCO) of 1000 g/mol was insufficient to retain the dissolved iron species (MWCO of 55.80 g/mol) and might be attributed to higher iron levels in the permeate in comparison to the feed in several experiments [50].

Additionally, the variation in post-filtration pH (from initially 3 up to 4.5) is observed across the 16 experimental runs (Appendix A.10). This phenomenon is likely associated with differences in the H_2O_2 dosage, catalyst loading, and membrane flux applied in each experiment. Variations in H_2O_2 concentration may influence the extent of oxidation reactions and the formation of intermediate products, while differences in catalyst dosage may affect the release of mineral species from the fly ash matrix. In addition, residual Fenton reactions may continue after filtration, potentially contributing to slight changes in the permeate pH. Therefore, the observed pH fluctuations are likely the result of the combined effects of these operational parameters.

Further statistical analysis was performed using JMP 18 software for all three responses: TOC removal, color removal, and iron residue. However, only the TOC removal analysis yielded statistically significant and interpretable results (The supplementary data of the JMP 18 software result on color removal and iron concentration are presented in Appendices A.7 and A.8). Therefore, this paper focuses exclusively on the JMP analysis of TOC removal, as it provided the most meaningful insights into the process. The statistical significance of the developed model was first evaluated using Analysis of Variance (ANOVA), as summarized in Figure 4a. The results indicate that the model is highly significant ($p = 0.0115$, $p < 0.05$), providing a reliable basis for further analysis of individual parameters. To pinpoint which specific factors drove this significance, an Effect Summary (Figure 4b) was subsequently employed. The significance of individual factors and their interactions with the response was evaluated. The combined influence of all factors on the response was analyzed at a 95% confidence interval, providing a comprehensive assessment of the process variables' impact on TOC removal efficiency. The LogWorth values in Figure 4 represent the *p*-values, with a higher LogWorth indicating greater statistical significance. Among the factors in the model, flux exhibits the highest LogWorth value (2.828), signifying its most probable significant impact. The rest of the factors, including the interaction between H_2O_2 and the catalyst, are considered to have a statistically insignificant impact on TOC removal, due to their *p*-values being greater than 0.05.

Furthermore, JMP 18 software is able to generate graphs that illustrate the correlation between actual and predicted responses. The correlation between predicted and actual data is crucial as it indicates how well a model replicates real-world outcomes. A strong correlation suggests reliable predictions, while a weak correlation implies potential inaccuracies, affecting decision-making. Assessing this correlation helps determine the model's predictive validity for these parameters. The predictive model for TOC removal yielded an R^2 value of 0.66 and an RMSE of 5.736 (Figure 5). While the model remains statistically significant (*p* value < 0.05), these values indicate that approximately 34% of the variance in TOC removal is not accounted for by the current experimental design. This lower degree of predictability is hypothesized to stem from the complex surface dynamics of the waste-derived FA-Fe_3O_4 catalyst. Additionally, the significant RMSE of 5.736 reflects residual error likely caused by uncaptured synergistic effects within the wastewater matrix and the inherent heterogeneity of the fly ash-based catalyst. This is supported by some

data points deviating from the regression line (solid red line running diagonally). This red line represents a perfect prediction, and the spread of data points around it shows a better model fit, with the shaded area indicating confidence intervals. These factors introduce non-linearities that exceed the predictive capacity of a standard second-order polynomial model, marking a boundary in the model's ability to predict absolute mineralization under varying operational conditions.

Source	DF	Sum of Squares	Mean Square	F Ratio
Model	4	715.8939	178.973	5.4381
Error	11	362.0204	32.911	Prob > F
C. Total	15	1077.9144		0.0115*

(**a**)

Source	Logworth	PValue
Flux(40,80)	2.828	0.00148
H2O2*Catalyst	0.781	0.16540
H2O2(10,30)	0.490	0.32347 ^
Catalyst(1,3)	0.419	0.38105 ^

(**b**)

Figure 4. Summary results from the JMP 18 software analysis: (**a**) ANOVA table result and (**b**) effect summary result. The value highlighted in red font (Figure 4a) within the "Prob > F" column explicitly indicates that the statistical parameter or model is highly significant ($p < 0.05$). The symbol (∗) (Figure 4b) denotes a cross interaction term between two operating parameters (H_2O and Catalyst), while the symbol (^) indicates individual main effects that are contained within that interaction effect listed above them.

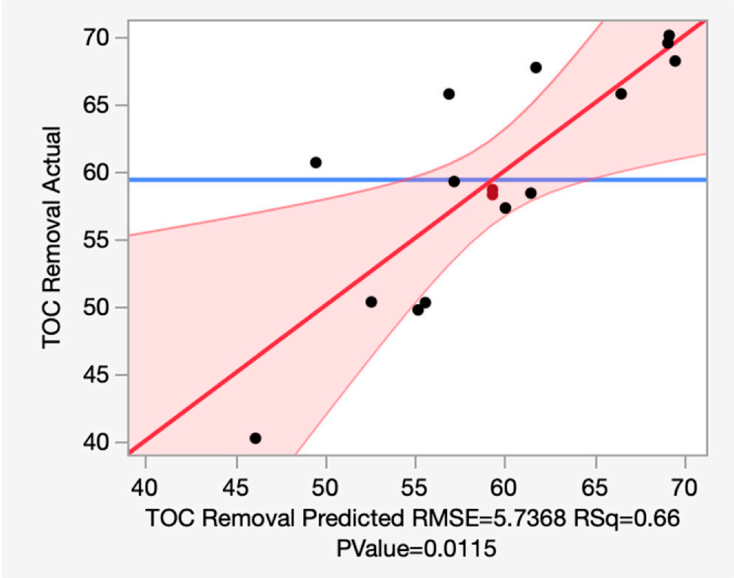

Figure 5. The plot of the experimental results vs the predicted results for TOC removal. The black circular markers represent the actual experimental data points, the solid red diagonal line denotes the ideal linear fit (y = x), the shaded red region signifies the 95% confidence curves for the model, and the horizontal solid blue line represents the overall sample mean of the response.

Additionally, JMP 18 software could produce a response surface plot for TOC removal from the interactions of each factor to visualize the factors' impact on TOC removal. Generally, the increasing number of factors resulted in greater TOC removal (Appendix A.9). However, the interaction model that excluded the flux factor yielded a slightly lower TOC removal efficiency than the configuration that accounted for flux. This shows that flux has a slightly more significant effect on the overall TOC removal. However, the significant lack of fit (0.0357) indicates that some systematic variation remains unexplained by the model. These results suggest that the model captures the main response trend and is sufficient for identifying flux as the most probable controlling parameter, although additional complexity in the system is not fully described by the current model.

Furthermore, to ensure the statistical validity and adequacy of the regression model, a residual diagnostic analysis was performed using JMP 18 software. The Residual by Predicted Plot displayed (Appendix A.11) a highly random distribution of error terms across the predicted TOC removal spectrum, successfully confirming homoscedasticity. Furthermore, evaluation of the Studentized Residuals revealed that all 16 experimental runs fell well within the 95% simultaneous Bonferroni limits (between −4 and +4), mathematically substantiating that the dataset contains no statistical outliers. The internal validation of this model was achieved via the built-in replicated center points within the factorial matrix. Combined with the robust overall model significance ($p = 0.0115$), these diagnostics verify that the empirical framework is statistically adequate and internally consistent for explaining the process trend within the evaluated experimental boundaries.

3.3. Membrane Performance: Multiple Filtration Cycles of Hybrid Fenton–Membrane and Energy Consumption

The hybrid configuration was designed as a single treatment unit to combine heterogeneous Fenton and membrane filtration. In this setup, the membrane's definitive role is the retention of the heterogeneous catalyst of FA-Fe_3O_4. Although the specific removal efficiency of the membrane alone was not isolated in this study, the overall performance of the hybrid process was captured by the statistical model ($p = 0.0115$, Figure 4a). The high significance of flux in the Effect Summary (LogWorth 2.828, Figure 4b) emphasizes that the filtration dynamics statistically have the most influence on the system's efficiency, impacting both pollutant removal and the energy intensity of the process.

The specific energy consumption (SEC) was calculated for various membrane filtration fluxes, as detailed in Appendix A.4. The analysis reveals an inverse relationship between flux and the energy requirement; specifically, operating at fluxes of 40, 60, and 80 LMH required 800, 500, and 400 kWh/m^3, respectively. This trend is attributed to the assumption that the pump is operating at a constant power supply of 40 watts across all flux variations, whereby higher fluxes achieve a greater permeate volume per unit of time, thus reducing the energy consumed per cubic meter of treated water. These results suggest that higher membrane fluxes significantly reduce the energy intensity of the filtration process within the tested range. This energy consumption can be considered relatively high compared to those reported for other nanofiltration (NF) membrane processes, which typically range from 0.56 to 10.5 kWh/m^3 [51,52]. This high energy consumption is an artifact of bench-scale limitations, driven by pump overhead, lower capacity operation, and a tiny membrane surface area. The applied flow rate (0.05 L/h) operates at the very low end of the pump's capacity. Because the pump suffers from high constant baseline overheads, it continuously draws its full nominal power of 40 W regardless of how low the flow rate is set. This severely diminishes its mechanical efficiency at this scale. The effective membrane area is extremely small, and the resulting filtrate volume is inherently minute (0.0125). Dividing the fixed energy input by this microscopic volume mathematically escalates the SEC.

Furthermore, in this study, membrane performance analysis was conducted by observation of the filtration curves and a comparison of membrane permeability decline (calculated from Equation (2)) with the specific filtered volume (Vsp). Filtration curve analysis was carried out on all experiments and classified based on flux variations of 40, 60, and 80 LMH (Figure 6). The resulting graphs show a comparison of filtration curves for each flux group based on the design of experiments 1 to 16 (See Table 3). Comparing the performance at different fluxes (Figure 6), all three different fluxes exhibited a decreasing trend in permeability at certain Vsp values. In general, higher filtration flux resulted from a higher filtered specific volume. For instance, at 80 LMH, the four-cycle filtration process was operated until a specific filtered volume of ± 100 L/m^2 was obtained. On the other hand, the lowest flux of 40 LMH resulted in a smaller specific volume of ± 50 L/m^2. Therefore, one might consider that the comparison of the performance of different fluxes could not be conducted. However, a comparison within a similar flux might explain the performance behavior with the other mentioned operation factors and parameters. Additionally, this study has shown that high flux also results in better permeate quality due to the formation of an additional filtration layer. On the other hand, the significant decline in membrane permeability indicates the occurrence of internal blocking. According to the literature, this type of fouling contributes to irreversible fouling [53]. This type of fouling can affect the lifespan of the membrane and increase costs in the long-term operation. It could be explained by the relatively high-pressure requirement (± 2 bar) for the highest flux applied of 80 LMH, whereas the highest pressures recorded for 60 LMH and 40 LMH are 0.5 bar and 0.1 bar, respectively.

Specifically, for the filtration runs conducted at a constant flux of 40 LMH, four distinct experiments can be seen in Figure 6a. From the figure, it can be seen that in the first filtration cycle, experiment 1 (H_2O_2 at 10 mL/L and a catalyst concentration of 1000 mg/L) and experiment 3 (H_2O_2 at 10 mL/L and a catalyst concentration of 3000 mg/L) exhibited comparable and stronger membrane fouling with permeabilities of 0.85 at the end. Furthermore, less membrane fouling was observed during experiment 2 (H_2O_2 at 30 mL/L and a catalyst concentration of 1 g/L), with an end permeability of 0.93, and experiment 4 (H_2O_2 at 30 mL/L and a catalyst concentration of 3000 mg/L), with an end permeability of 0.88. During filtration in the 2nd cycle, the initial permeabilities for all four experiments were found to be similar and could not be achieved. This indicates that mechanical irreversible fouling occurred. Different from the first filtration cycle, the later filtration cycle (2nd–4th) revealed a comparable membrane fouling propensity. In correlation with process efficiency (Table 3), it could be seen that the influence of different concentrations of hydrogen peroxide and catalyst were found to be insignificant to membrane fouling propensity during filtration at a flux of 40 LMH. This is based on the overlapping profiles of the permeability curves across different experimental conditions operating in the same flux of 40 LMH (Figure 6a). All experiments exhibited a similar final normalized permeability (ranging between 0.9 and 0.7) and a consistent decline pattern.

Multiple-cycle membrane filtration was performed at a flux of 60 LMH. Different from the other two variations of flux, the filtration cycle at a flux of 60 LMH was categorized into six different conditions (see Table 3). A comparison of performance was further conducted at a flux of 60 LMH (See Figure 6c). In general, a severe membrane performance with an end permeability of 0,6 was observed during filtration in experiment 12 (H_2O_2 at 20 mL/L and a catalyst concentration of 3420 mg/L). In parallel, the other experiment revealed a comparable membrane fouling performance despite the concentrations of hydrogen peroxide and catalyst. Similar to filtration at 40 LMH, the influence of hydrogen peroxide and catalyst concentration on membrane fouling could not be clearly identified. The

mentioned experiment 12 was found to have severe membrane fouling with a comparable high concentration of hydrogen peroxide and the highest concentration of catalyst.

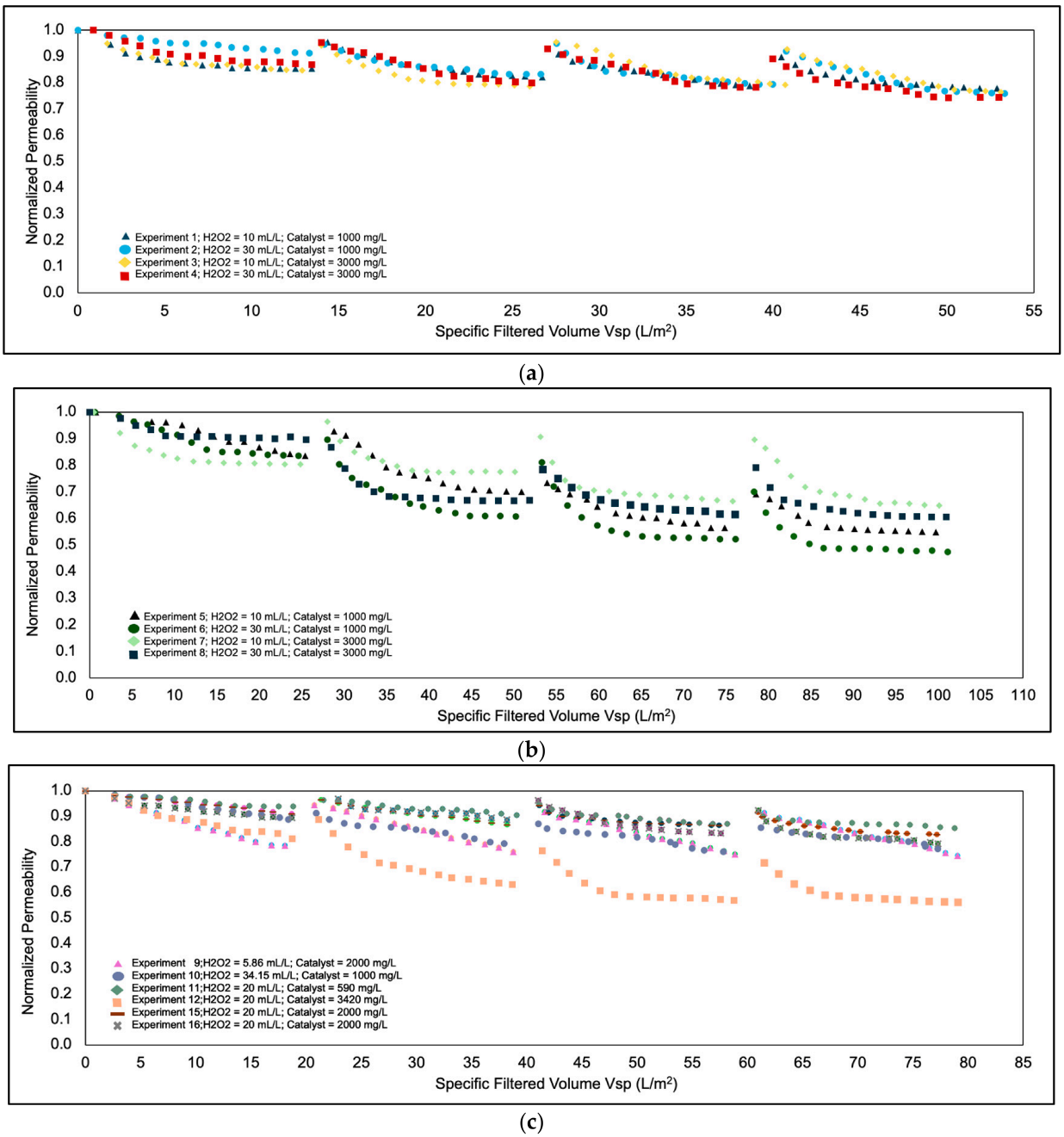

Figure 6. Multiple filtration cycles at the following fluxes: (**a**) 40 LMH, (**b**) 80 LMH, and (**c**) 60 LMH.

Further observation of membrane performance was conducted at a constant flux of 80 LMH. Different from 40 and 60 LMH, an interesting membrane fouling behavior was seen in this filtration experiment. The first filtration cycle exhibited a relatively comparable performance of experiment 5 (H_2O_2 at 10 mL/L and a catalyst concentration of 1000 mg/L), experiment 6 (H_2O_2 at 30 mL/L and a catalyst concentration of 1000 mg/L), and experiment 8 (H_2O_2 at 30 mL/L and a catalyst concentration of 3000 mg/L) with an end permeability of around 0.85 (Figure 6b). However, a more pronounced decline in permeability was observed in experiment 7 (H_2O_2 at 10 mL/L and a catalyst concentration of 3000 mg/L), reaching an end permeability of 0.78. In the second filtration cycle, a different membrane fouling propensity was observed. Due to mechanical membrane backwashing, the initial

permeability of the second filtration cycle was found to vary. Experiments 5 and 7 exhibited similarly high initial permeabilities at 0.9, in comparison to experiments 6 and 8, each with an initial lower permeability of 0.81. Despite similar initial permeabilities in the 2nd cycle for experiments 5 and 7, as well as 6 and 8, membrane permeability decline at the end of the cycle resulted in different end permeabilities. Interestingly, data from experiment 7 revealed a more tempered permeability decline compared to the other configurations, concluding with a final permeability of 0.79. In contrast, experiment 6 exhibited a more severe decline in permeability, dropping to a final value of 0.6. Regarding experiment 7, an opposite performance trend associated with severe membrane fouling was noted when compared to its first filtration cycle. In the 3rd filtration cycle, the membrane performance of experiment 6 revealed severe membrane fouling with an end permeability of 0.55, whereas experiment 7 experienced less intensive fouling, maintaining a higher value of 0.67. Meanwhile, experiment 5 and 8 exhibited comparable end permeabilities of 0.62. In the last filtration cycle (4th cycle), experiment 6 experienced the most severe membrane permeability decline compared to the other experimental conditions, with 0.5 as the end permeability. On the other hand, the other experiments showed stable performance with end permeabilities of 0.66, 0.61, and 0.61 for experiments 5, 7, and 8, respectively.

It could be suggested that the higher hydrogen peroxide levels resulted in a more severe membrane fouling. However, relating it to the pollutant retention (see Table 3), the severe membrane fouling is attributed to the lower iron concentration on the permeate side. This might indicate that the hydrogen peroxide successfully oxidizes iron despite different catalyst concentrations into other forms that are able to be retained by the membrane. The oxidized iron was changed into another form, which accelerated the formation of a cake layer on the membrane surface. The cake layer completely blocks the membrane pores [54], preventing any further increase in transmembrane pressure and resulting in a less rapid decline in permeability. In contrast, the experiments with lower catalyst dosages showed higher initial permeabilities and a higher rate of permeability decline, consistent with the findings of another study [53]. The consistent reduction in permeability across all experiments signifies the occurrence of membrane fouling. This phenomenon is characterized by dynamic interactions between organic and inorganic contaminants and the membrane surface. The deposit of contaminants on the membrane surface is visible as it is captured in Appendix A.3. The accumulation of foulants within the membrane pores obstructs fluid flow and results in a higher transmembrane pressure to sustain a constant flux of 80 LMH. Such interactions progressively diminish the membrane's permeability [55].

By evaluating the comprehensive removal datasets across the varied operational parameters presented in Table 3, alongside the systematic assessment of membrane fouling behaviors discussed previously, a clear correlation between operating conditions and system responses can be established. To establish a sustainable trade-off between process economics, membrane longevity, and treatment efficiency, the objective function for process optimization was defined based on minimizing the operational inputs and fouling stress while maintaining adequate organic degradation. Consequently, the optimal operational conditions were identified to be a combination of operational conditions that consist of a flux of 40 LMH, 30 mL/L of H_2O_2, and 1000 mg/L of catalyst (Experiment 2). The selection of this specific run is heavily justified by techno-economic and structural considerations. Operating at the lowest boundaries for both flux (40 LMH) and catalyst dosage (1000 mg/L) significantly reduces chemical costs and mitigates hydraulic fouling pressure on the filtration layer. This is supported by the system's ability to maintain a stable normalized permeability above 0.7 after multiple cycles, compared to the severe permeability drops observed in other flux experiments. The high requirement of H_2O_2 concentration at 30 mL/L, is compensated by the lower catalyst and flux requirement. This ensured a highly

efficient organic pollutant degradation without compromising the physical stability of the ceramic membrane matrix. The requirement for a relatively high mass-based H_2O_2/TOC ratio (8.5:1, for 30 mL/L H_2O_2) is highly associated with the complex chemical matrix of winery wastewater. It consists of organic compounds, including polyphenols, tannins, and complex organic acids, which naturally act as radical scavengers [2].

Among the experimental runs conducted in this study, experiment 2 was identified as the optimal condition, yielding a TOC removal efficiency of approximately 70%, corresponding to a residual effluent TOC concentration of 586 mg/L. While this removal performance is indicative of a meaningful reduction in organic load, the resulting effluent concentration remains substantially above the permissible discharge thresholds established by several international regulatory frameworks, highlighting the gap between current treatment performance and compliance requirements. In South Korea, the Ministry of Environment (MOE) determined discharge limits of organic compounds in industrial wastewater, effective from 2022. Under this framework, the permissible TOC limit for industrial effluent discharge ranges from 25 to 75 mg/L depending on the receiving water body and facility classification [56]. Similarly, under the BAT-AELs established by Directive 2010/75/EU of the European Parliament and of the Council, the annual average TOC concentration in treated effluents generally ranges from 10 to 33 mg/L. These comparative findings collectively indicate that while the treatment system evaluated in this study demonstrates substantial organic load reduction, a single-stage treatment configuration is insufficient to achieve effluent quality that meets international discharge standards for direct release into surface water bodies.

4. Conclusions

Based on this study, there are several interesting findings related to a combined membrane–Fenton process:

- The augmentation of iron oxide with coal fly ash was able to be utilized as a Reuse material for the Fenton process.
- A sequence of 16 experiments planned according to a CCD design study demonstrated that the hybrid Fenton–membrane process was able to remove 90% of color and 70% of TOC. However, iron residue of up to 12 mg/L persisted in the membrane permeate in several cases due to the catalysts' leaching process. Pollutant removal was achieved through the combination of Fenton oxidation and membrane filtration operating parameters. Based on the multi-factorial analysis, flux was identified as the most critical factor influencing TOC removal (p = 0.00148), followed by the synergistic interaction between H_2O_2 and catalyst dosage in the heterogenous Fenton reaction. To achieve a balance between high treatment efficiency and membrane stability, the optimal operational conditions were determined to be a flux of 40 LMH, H_2O_2 30 mL/L, and 1000 mg/L of catalyst (experiment 2). Under these conditions, the system maintains a stable normalized permeability above 0.7 after multiple cycles while achieving high organic pollutant degradation.
- Further analysis using JMP 18 software identified flux as the most probable significant factor influencing the removal of TOC. Unfortunately, a lack of fit data prevented the development of a reliable predictive model to optimize the process parameters for enhanced color removal and iron residue modeling.
- In the hybrid heterogeneous Fenton and membrane filtration process, the lower flux filtration was found to result in less membrane fouling in comparison to higher flux filtration. Moreover, severe membrane fouling was related to better membrane retention and indicates a deposition of organic matter, iron, and fly ash during the filtration process. In practical applications, while the objective is to operate at the

highest possible flux with minimal fouling, this study demonstrates that a trade-off exists. As shown in Figure 6b,c, higher flux operations resulted in a more pronounced flux decline although it produced better permeate quality and quantity. This confirms that high-volume treatment targets must be balanced against the operational costs associated with membrane fouling and lifespan. Therefore, the application of the hybrid heterogeneous Fenton and membrane reactor needs to be adjusted to the scale of industrial wine wastewater production in order to determine the priorities of the treatment process.

- This research is limited to a laboratory-scale evaluation using a Central Composite Design (CCD) framework under the Design of Experiments (DoE) introduced by Kleppmann. The primary objective was to assess the hybrid system using a minimized number of experimental runs combined with statistical tools that successfully indicate the most probable factors affecting the system's performance. Additionally, because the investigation was designed to evaluate the hybrid process as one integrated treatment, the intermediate residual H_2O_2 concentration after the oxidation phase was not experimentally determined, representing an analytical boundary of this work. Within this context, the statistical analysis derived from the software serves primarily as a macro-performance indicator for trend identification, and a multitude of other dynamic environmental variables must be accounted for in real-world applications.
- As a lab-scale study, the operational behaviour of the laboratory equipment—specifically the auxiliary feed pumps and low-volume fluid transport lines—differs significantly from full-scale industrial facilities in terms of mechanical efficiency, hydraulic shear, and power consumption scaling.
- To further enhance the holistic viability of this treatment method, future efforts should move beyond the lab scale to investigate dynamic feed pulsing strategies, precise energy-use modelling for industrial pumps, advanced surface modifications of the coal fly ash protective matrix to systematically suppress long-term membrane fouling, and further treatment for the effluent pH and iron concentration adjustments. Accordingly, systematic assessments of catalyst reusability and their extended chemical stability across sequential runs should be prioritized in subsequent studies.

Author Contributions: Conceptualization, F.M.K., S.L., S.A., L.L. and S.P.; methodology, F.M.K., S.L., S.A., L.L. and S.P.; software, F.M.K.; validation, F.M.K. and S.A.; formal analysis, F.M.K., S.L. and S.A.; investigation, F.M.K.; resources, F.M.K., L.L. and S.P.; data curation, F.M.K. and S.L.; writing—original draft preparation, F.M.K.; writing—review and editing, F.M.K., S.L., L.L. and S.P.; visualization, F.M.K., S.L., L.L. and S.P.; supervision, S.L. and S.P.; project administration, F.M.K. and S.L.; funding acquisition, F.M.K. and S.L. All authors have read and agreed to the published version of the manuscript.

Funding: This research was funded by the Directorate of Research and Development, Universitas Indonesia under Hibah PUTI 2023 (Grant No. NKB-543/UN2.RST/HKP.05.00/2023).

Data Availability Statement: The raw data supporting the conclusions of this article will be made available by the authors on request.

Conflicts of Interest: The authors declare no conflicts of interest.

Appendix A

Appendix A.1

The characteristics of greywater obtained from a domestic wastewater treatment plant (WWTP) in South Jakarta, which was subsequently used as a constituent in the preparation of synthetic winery wastewater.

Table A1. Wastewater (greywater) characteristics.

Parameter	Unit	Value
pH	-	6.5
COD	mg/L	55
Total Iron	mg/L	2
Color	Pt-Co	20

Appendix A.2

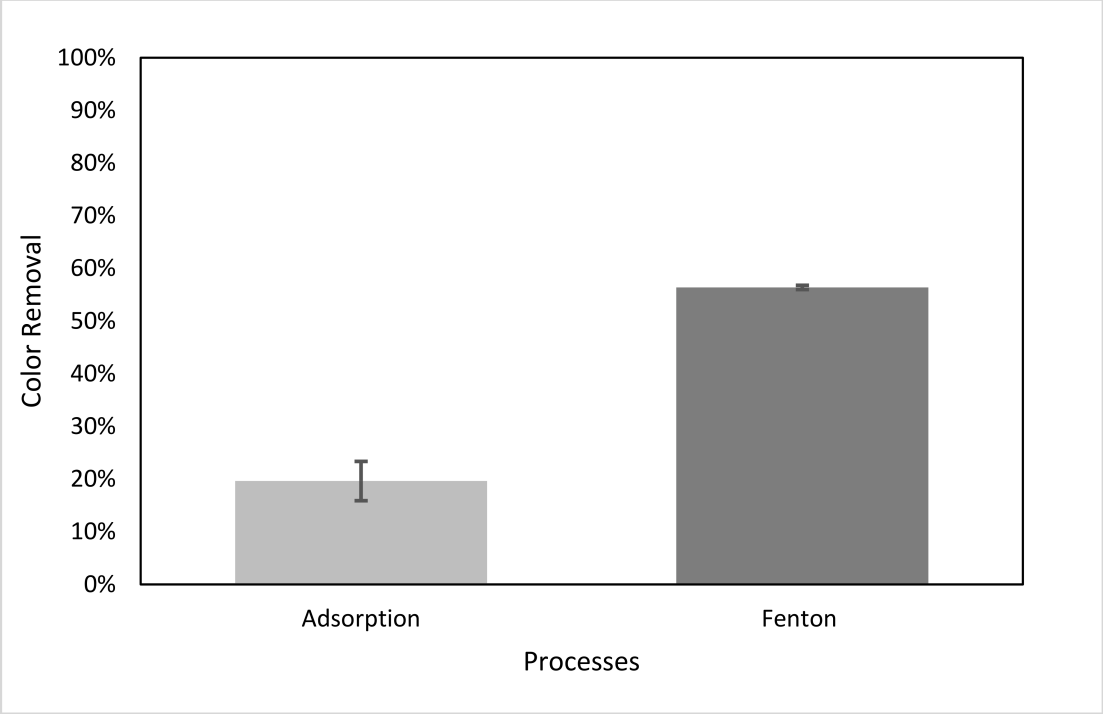

Figure A1. A total of 2 g/L FA-Fe_3O_4 performance in adsorption (absence of H_2O_2) and Fenton.

Appendix A.3

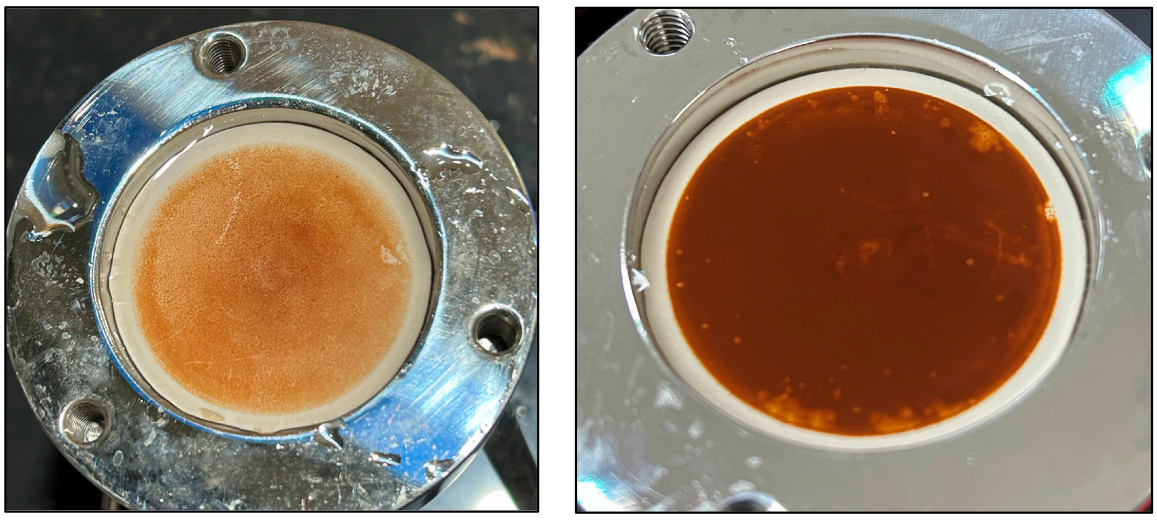

(**a**) (**b**)

Figure A2. Cake Layer on membrane surface at different filtration fluxes: (**a**) 40 LMH and (**b**) 80 LMH.

Appendix A.4

Table A2. Pump Operational Parameters During Filtration.

Pump Information		
Brand	longer	
type	BT 100-1F	
power supply	40	watt
Filtration duration		
15		mins
0.25		hour
Energy used		
10		Wh
0.01		kWh

Table A3. Specific energy consumption calculation.

Flux (L/m^3/h)	Pump Flow Rate (L/h)	Volume During 15 min Filtration m^3	Specific Energy Consumption (kWh/m^3)
40	0.05	0.0000125	800
60	0.08	0.00002	500
80	0.1	0.000025	400

Appendix A.5

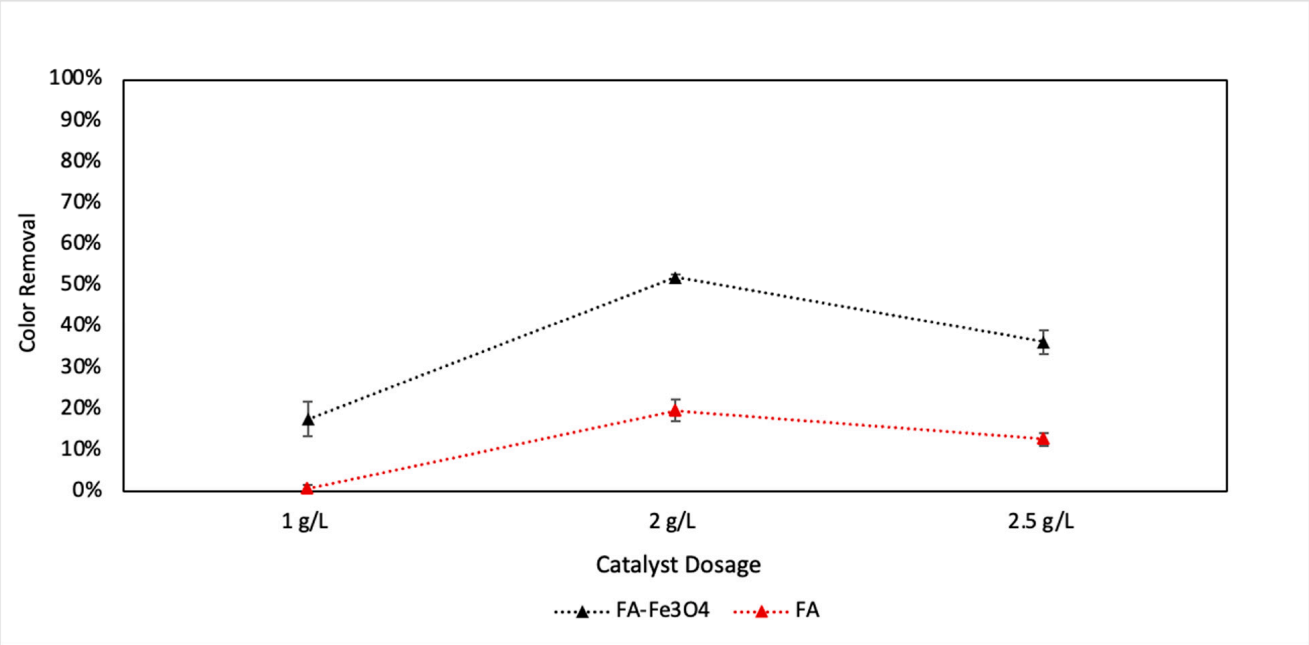

Figure A3. Comparison of the performance of FA and FA-Fe_3O_4 in heterogenous Fenton reaction with H_2O_2:COD 1:1.

Appendix A.6

Table A4. PSA result of FA-Fe_3O_4: Frequency Cumulative.

Diameter (nm)	Frequency (%)	Frequency Cumulative (%)
43	0	0
47	0	0
51	19.6	19.6
56	20.9	40.5
61	18.6	59.1
66	14.6	73.7
72	10.4	84.1
79	6.9	91.0
86	4.2	95.2
93	2.4	97.6
102	1.3	98.9
111	0.7	99.6
121	0.3	99.9
132	0.1	100.0
143	0	100.0
156	0	100.0

Table A5. PSA result of FA-Fe_3O_4: Contin Analysis.

Peak	Diameter (nm)	St.Dev
1	64.2	12.7
2	2073.50	442.7
3	0	0
4	0	0
5	0	0
Average	64.5	29.4

Table A6. PSA result of FA-Fe_3O_4: Cumulants Result.

Diameter (d)	2633.2	nm
Polydispersity Index (P.I)	1.024	
Diffusion Const	1.868×10^9	cm^2/s

Appendix A.7

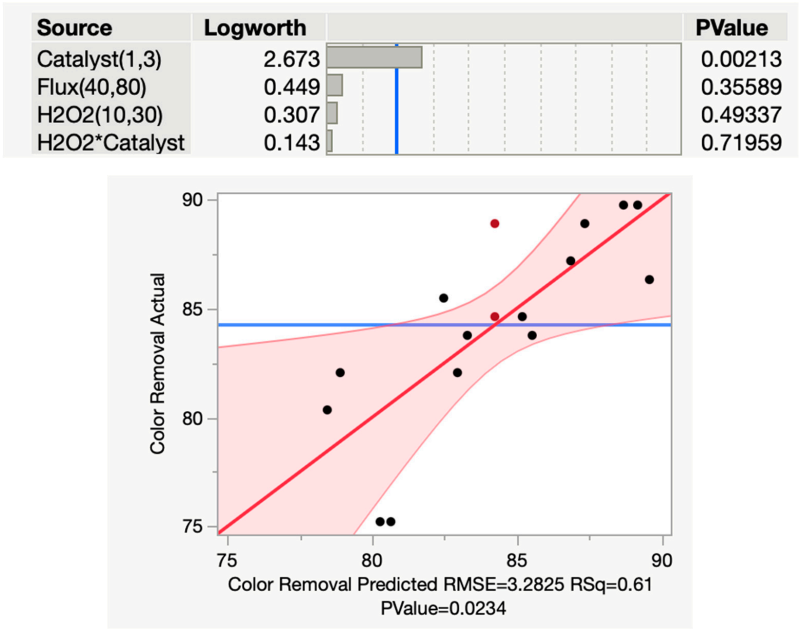

Figure A4. JMP 18 result for color removal. The symbol (∗) denotes a cross interaction term between two operating parameters (H_2O and Catalyst). The black circular markers represent the actual experimental data points, the solid red diagonal line denotes the ideal linear fit (y = x), the shaded red region signifies the 95% confidence curves for the model, and the horizontal solid blue line represents the overall sample mean of the response.

Appendix A.8

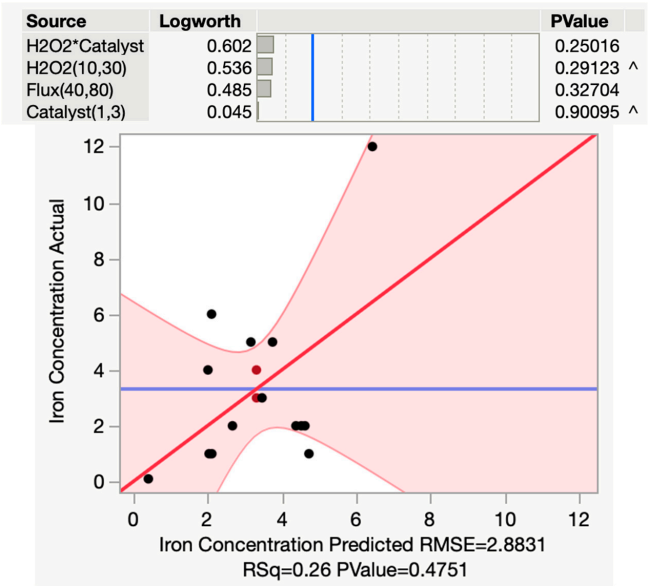

Figure A5. JMP 18 result for iron concentration. The symbol (∗) denotes a cross interaction term between two operating parameters (H_2O and Catalyst), while the symbol (^) indicates individual main effects that are contained within that interaction effect listed above them. The black circular markers represent the actual experimental data points, the solid red diagonal line denotes the ideal linear fit (y = x), the shaded red region signifies the 95% confidence curves for the model, and the horizontal solid blue line represents the overall sample mean of the response.

Appendix A.9

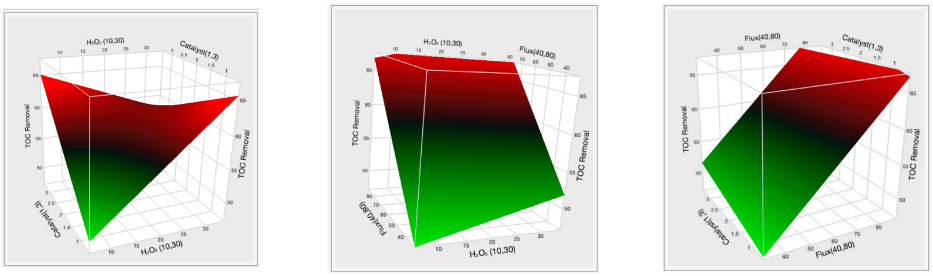

(**a**) (**b**) (**c**)

Figure A6. Response surface plot for TOC removal: (**a**) H_2O_2 vs. Catalyst, (**b**) H_2O_2 vs. Flux, and (**c**) Flux vs. Catalyst [3]. The continuous color gradients illustrate smooth, progressive transitions in TOC degradation efficiency across the experimental boundaries, indicating a predictable empirical trend.

Appendix A.10

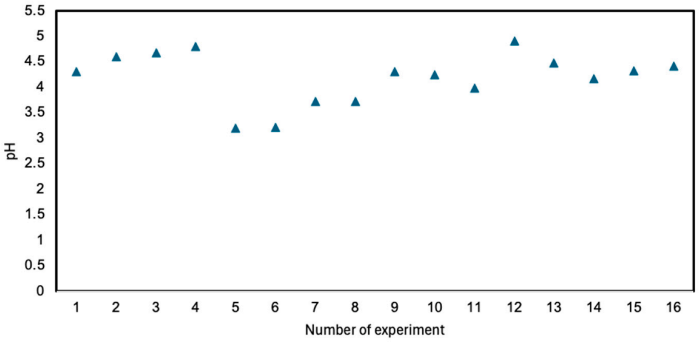

Figure A7. pH Changes in permeate pH after the filtration process across the 16 experimental runs.

Appendix A.11

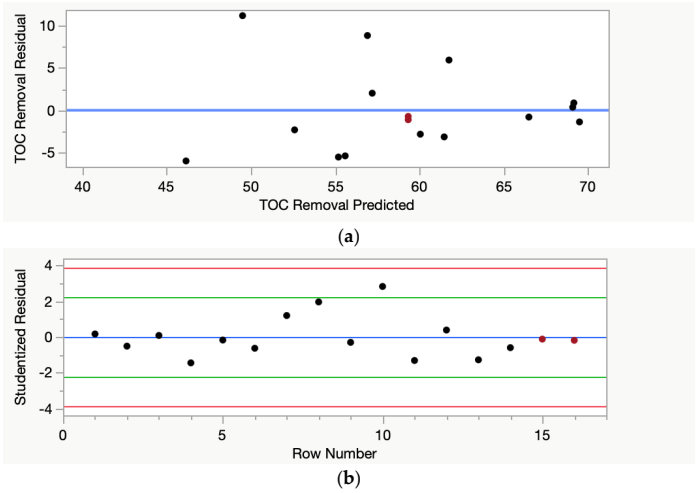

(**a**)

(**b**)

Figure A8. JMP 18 Software analysis (**a**) Residuals by predicted plot (**b**) studentized plot analysis. The black circular markers represent individual residuals, while the horizontal solid blue line denotes the zero-residual baseline. The single red marker at the center coordinates signifies the unbiased mean value of the residuals (0.00). Studentized residual plot for outlier screening. The black circular markers represent the studentized residual values. The two horizontal solid red lines establish the statistical control boundaries, confirming the absolute absence of critical outliers in the data.

References

1. Sudhinaraset, M.; Wigglesworth, C.; Takeuchi, D. Social and Cultural Contexts of Alcohol Use: Influences in a Social-Ecological Framework. *Alcohol Res.* **2016**, *38*, 35–45. [CrossRef] [PubMed]
2. Latessa, S.H.; Hanley, L.; Tao, W. Characteristics and practical treatment technologies of winery wastewater: A review for wastewater management at small wineries. *J. Environ. Manag.* **2023**, *342*, 118343. [CrossRef] [PubMed]
3. Johnson, M.B.; Mehrvar, M. Winery wastewater management and treatment in the Niagara Region of Ontario, Canada: A review and analysis of current regional practices and treatment performance. *Can. J. Chem. Eng.* **2020**, *98*, 5–24. [CrossRef]
4. Ioannou, L.A.; Puma, G.L.; Fatta-Kassinos, D. Treatment of winery wastewater by physicochemical, biological and advanced processes: A review. *J. Hazard. Mater.* **2015**, *286*, 343–368. [CrossRef] [PubMed]
5. Ippolito, N.M.; Zueva, S.B.; Ferella, F.; Corradini, V.; Baturina, E.V.; Vegliò, F. Treatment of waste water from a winery with an advanced oxidation process (AOP). *IOP Conf. Ser. Earth Environ. Sci.* **2021**, *640*, 062025. [CrossRef]
6. Ngwenya, N.; Gaszynski, C.; Ikumi, D. A review of winery wastewater treatment: A focus on UASB biotechnology optimisation and recovery strategies. *J. Environ. Chem. Eng.* **2022**, *10*, 108172. [CrossRef]
7. Bolzonella, D.; Papa, M.; Da Ros, C.; Muthukumar, L.A.; Rosso, D. Winery wastewater treatment: A critical overview of advanced biological processes. *Crit. Rev. Biotechnol.* **2019**, *39*, 489–507. [CrossRef] [PubMed]
8. Malandra, L.; Wolfaardt, G.; Zietsman, A.; Viljoen-Bloom, M. Microbiology of a biological contactor for winery wastewater treatment. *Water Res.* **2003**, *37*, 4125–4134. [CrossRef] [PubMed]
9. Bories, A.; Sire, Y. Impacts of Winemaking Methods on Wastewaters and their Treatment. *S. Afr. J. Enol. Vitic.* **2010**, *31*, 38. [CrossRef]
10. Andreottola, G.; Foladori, P.; Ziglio, G. Biological treatment of winery wastewater: An overview. *Water Sci. Technol.* **2009**, *60*, 1117–1125. [CrossRef] [PubMed]
11. Jain, B.; Singh, A.K.; Kim, H.; Lichtfouse, E.; Sharma, V.K. Treatment of organic pollutants by homogeneous and heterogeneous Fenton reaction processes. *Environ. Chem. Lett.* **2018**, *16*, 947–967. [CrossRef]
12. Mosteo, R.; Ormad, P.; Mozas, E.; Sarasa, J.; Ovelleiro, J.L. Factorial experimental design of winery wastewaters treatment by heterogeneous photo-Fenton process. *Water Res.* **2006**, *40*, 1561–1568. [CrossRef] [PubMed]
13. Jorge, N.; Teixeira, A.R.; Silva, S.; Pirra, A.; Peres, J.A.; Lucas, M.S. Homogeneous vs. Heterogeneous Photo-Fenton Processes in the Treatment of Winery Wastewater. *Eng. Proc.* **2023**, *56*, 288. [CrossRef]
14. Adityosulindro, S.; Julcour, C.; Barthe, L. Heterogeneous Fenton oxidation using Fe-ZSM5 catalyst for removal of ibuprofen in wastewater. *J. Environ. Chem. Eng.* **2018**, *6*, 5920–5928. [CrossRef]
15. Xu, J.; Long, Y.; Shen, D.; Feng, H.; Chen, T. Optimization of Fenton treatment process for degradation of refractory organics in pre-coagulated leachate membrane concentrates. *J. Hazard. Mater.* **2017**, *323*, 674–680. [CrossRef] [PubMed]
16. Plakas, K.V.; Mantza, A.; Sklari, S.D.; Zaspalis, V.T.; Karabelas, A.J. Heterogeneous Fenton-like oxidation of pharmaceutical diclofenac by a catalytic iron-oxide ceramic microfiltration membrane. *Chem. Eng. J.* **2019**, *373*, 700–708. [CrossRef]
17. Zhang, X.; Zhang, Q.; Yang, T.; Li, Y.; Li, J.; Yu, T.; Qu, C. Research progress of heterogeneous Fenton catalyst for organic wastewater treatment. *IOP Conf. Ser. Earth Environ. Sci.* **2021**, *651*, 042025. [CrossRef]
18. Liu, X.; Yao, Y.; Lu, J.; Zhou, J.; Chen, Q. Catalytic activity and mechanism of typical iron-based catalysts for Fenton-like oxidation. *Chemosphere* **2023**, *311*, 136972. [CrossRef] [PubMed]
19. Hussain, S.; Aneggi, E.; Goi, D. Catalytic activity of metals in heterogeneous Fenton-like oxidation of wastewater contaminants: A review. *Environ. Chem. Lett.* **2021**, *19*, 2405–2424. [CrossRef]
20. Wang, N.; Sun, X.; Zhao, Q.; Yang, Y.; Wang, P. Leachability and adverse effects of coal fly ash: A review. *J. Hazard. Mater.* **2020**, *396*, 122725. [CrossRef] [PubMed]
21. Ghazali, M.; Kaushal, O.P. Characteristics of Fly Ash from Thermal Power Plants and its Management along with Settling Pond Design. *Int. J. Eng. Res. Sci.* **2015**, *1*, 24–32.
22. Niveditha, S.V.; Gandhimathi, R. Flyash augmented Fe_3O_4 as a heterogeneous catalyst for degradation of stabilized landfill leachate in Fenton process. *Chemosphere* **2020**, *242*, 125189. [CrossRef] [PubMed]
23. Parker, J. *Fly Ash: Properties, Analysis and Performance*; CRC Press: Boca Raton, FL, USA, 2017.
24. Wang, N.; Zhao, Q.; Li, Q.; Zhang, G.; Huang, Y. Degradation of polyacrylamide in an ultrasonic-Fenton-like process using an acid-modified coal fly ash catalyst. *Powder Technol.* **2020**, *369*, 270–278. [CrossRef]
25. Wang, N.; Li, L.; Zhang, Y.; Han, Y.; Li, Z. Fe_2O_3/coal fly ash Fenton-like catalyst for the elimination of organic pollutants in wastewater: Kinetic, mechanism, and application feasibility. *J. Environ. Chem. Eng.* **2023**, *11*, 110961. [CrossRef]
26. Zhao, Y.; Wang, F.; Yang, J.; Yang, F.; Deng, X.; Li, J.; Liu, W.; Sun, L. Synthesis of coal fly ash-based heterogeneous Fenton catalyst for bisphenol a removal: Performances and proposed mechanism. *Vacuum* **2023**, *212*, 112054. [CrossRef]
27. Saechan, C.; Thawornpan, P.; Thanapongpichat, S.; Hongmanee, S.; Srinoun, K.; Win Tun, A.; Tansila, N.; Jumpathong, W.; Buncherd, H. Degradation of Methylene Blue Using Fly Ash as a Heterogeneous Fenton Catalyst. *Anal. Lett.* **2023**, *56*, 2099–2112. [CrossRef]

28. Shehata, N.; Egirani, D.; Olabi, A.G.; Inayat, A.; Abdelkareem, M.A.; Chae, K.J.; Sayed, E.T. Membrane-based water and wastewater treatment technologies: Issues, current trends, challenges, and role in achieving sustainable development goals, and circular economy. *Chemosphere* **2023**, *320*, 137993. [CrossRef] [PubMed]
29. Othman, N.H.; Alias, N.H.; Fuzil, N.S.; Marpani, F.; Shahruddin, M.Z.; Chew, C.M.; David Ng, K.M.; Lau, W.J.; Ismail, A.F. A Review on the Use of Membrane Technology Systems in Developing Countries. *Membranes* **2021**, *12*, 30. [CrossRef] [PubMed]
30. Ho, D.P.; Vigneswaran, S.; Ngo, H.H. Photocatalysis-membrane hybrid system for organic removal from biologically treated sewage effluent. *Sep. Purif. Technol.* **2009**, *68*, 145–152. [CrossRef]
31. Real, F.J.; Benitez, F.J.; Acero, J.L.; Roldan, G. Combined chemical oxidation and membrane filtration techniques applied to the removal of some selected pharmaceuticals from water systems. *J. Environ. Sci. Health Part A* **2012**, *47*, 522–533. [CrossRef] [PubMed]
32. Aydiner, C.; Mert, B.K.; Dogan, E.C.; Yatmaz, H.C.; Dagli, S.; Aksu, S.; Tilki, Y.M.; Goren, A.Y.; Balci, E. Novel hybrid treatments of textile wastewater by membrane oxidation reactor: Performance investigations, optimizations and efficiency comparisons. *Sci. Total Environ.* **2019**, *683*, 411–426. [CrossRef] [PubMed]
33. He, Y.; He, M.; Liu, T.; Lu, D.; Zhou, Z.; Ma, J. Adsorption-enhanced Fenton catalytic membrane for high-efficiency, high-quality drinking water treatment. *J. Hazard. Mater.* **2025**, *483*, 136632. [CrossRef] [PubMed]
34. Ganiyu, S.O.; van Hullebusch, E.D.; Cretin, M.; Esposito, G.; Oturan, M.A. Coupling of membrane filtration and advanced oxidation processes for removal of pharmaceutical residues: A critical review. *Sep. Purif. Technol.* **2015**, *156*, 891–914. [CrossRef]
35. Lan, Y.; Causserand, C.; Barthe, L. Practical insights into ultrasound-assisted heterogeneous Fenton membrane reactors for water treatment. *J. Water Process Eng.* **2022**, *45*, 102523. [CrossRef]
36. Uman, A.E.; Bair, R.A.; Yeh, D.H. Direct Membrane Filtration of Wastewater: A Comparison between Real and Synthetic Wastewater. *Water* **2024**, *16*, 405. [CrossRef]
37. Gruskevica, K.; Mezule, L. Cleaning Methods for Ceramic Ultrafiltration Membranes Affected by Organic Fouling. *Membranes* **2021**, *11*, 131. [CrossRef] [PubMed]
38. Kleppmann, W. *Versuchsplanung: Produkte und Prozesse Optimieren*; Carl Hanser Verlag GmbH & Co. KG: Munich, Germany, 2016. [CrossRef]
39. Bhatt, A.; Priyadarshini, S.; Mohanakrishnan, A.A.; Abri, A.; Sattler, M.; Techapaphawit, S. Physical, chemical, and geotechnical properties of coal fly ash: A global review. *Case Stud. Constr. Mater.* **2019**, *11*, e00263. [CrossRef]
40. Juda-Rezler, K.; Kowalczyk, D. Size Distribution and Trace Elements Contents of Coal Fly Ash from Pulverized Boilers. *Pol. J. Environ. Stud.* **2013**, *22*, 25–40.
41. Ocampo-Gaspar, M.; Cano-Guzmán, C.F.; Payan-Martínez, L.F.; González-Reyes, L.; Hernández-Pérez, I.; Garibay-Febles, V.; Pérez-Orozco, J.P.; Cabrera-Lara, L.I.; Ramón-García, M.L.; Galicia-Luis, L.; et al. Sizing the Fenton's catalyst. *J. Photochem. Photobiol. A Chem.* **2018**, *353*, 527–535. [CrossRef]
42. Barb, W.G.; Baxendale, J.H.; George, P.; Hargrave, K.R. Reactions of ferrous and ferric ions with hydrogen peroxide. Part I.—The ferrous ion reaction. *Trans. Faraday Soc.* **1951**, *47*, 462–500. [CrossRef]
43. Almazán-Sánchez, P.T.; Linares-Hernández, I.; Martínez-Miranda, V.; Lugo-Lugo, V.; de Oca, R.M.G.F.-M. Wastewater treatment of methyl methacrylate (MMA) by Fenton's reagent and adsorption. *Catal. Today* **2014**, *220–222*, 39–48. [CrossRef]
44. Ibrar, I.; Naji, O.; Sharif, A.; Malekizadeh, A.; Alhawari, A.; Alanezi, A.A.; Altaee, A. A Review of Fouling Mechanisms, Control Strategies and Real-Time Fouling Monitoring Techniques in Forward Osmosis. *Water* **2019**, *11*, 695. [CrossRef]
45. Bugge, T.V.; Jørgensen, M.K.; Christensen, M.L.; Keiding, K. Modeling cake buildup under TMP-step filtration in a membrane bioreactor: Cake compressibility is significant. *Water Res.* **2012**, *46*, 4330–4338. [CrossRef] [PubMed]
46. Petrinic, I.; Christensen, M.L.; Basitere, M.; Buksek, H. Exploring the impact of fouling on permeate flux and quality in ceramic ultrafiltration after treating poultry wastewater, and strategies for effective modelling and mitigation. *J. Water Process Eng.* **2023**, *56*, 104348. [CrossRef]
47. Krupińska, I. Application of Fenton's Reaction for Removal of Organic Matter from Groundwater. *Molecules* **2024**, *29*, 5150. [CrossRef] [PubMed]
48. Eroğlu, H.A.; Akbal, F. Enhancing textile wastewater reuse: Integrating Fenton oxidation with membrane filtration. *J. Environ. Manag.* **2025**, *379*, 124873. [CrossRef] [PubMed]
49. Borgatta, J.; Paskavitz, A.; Kim, D.; Navea, J.G. Comparative evaluation of iron leach from different sources of fly ash under atmospherically relevant conditions. *Environ. Chem.* **2016**, *13*, 902–912. [CrossRef]
50. Zhang, Y.; Liu, C.; Li, Y.; Song, L.; Yang, J.; Zuo, R.; Li, J.; Teng, Y.; Wang, J. Spectroscopic Characteristics and Speciation Distribution of Fe(III) Binding to Molecular Weight-Dependent Standard Pahokee Peat Fulvic Acid. *Int. J. Environ. Res. Public Health* **2022**, *19*, 7838. [CrossRef] [PubMed]
51. Meiramkulova, K.; Devrishov, D.; Zhumagulov, M.; Arystanova, S.; Karagoishin, Z.; Marzanova, S.; Kydyrbekova, A.; Mkilima, T.; Li, J. Performance of an Integrated Membrane Process with Electrochemical Pre-Treatment on Poultry Slaughterhouse Wastewater Purification. *Membranes* **2020**, *10*, 256. [CrossRef] [PubMed]

52. Xin, G.; Lopes, M.P.; Crespo, J.G.; Rusten, B. A continuous nanofiltration + evaporation process for high strength rubber wastewater treatment and water reuse. *Sep. Purif. Technol.* **2013**, *119*, 19–27. [CrossRef]
53. Abdelrasoul, A.; Doan, H.; Lohi, A. Fouling in Membrane Filtration and Remediation Methods. In *Mass Transfer—Advances in Sustainable Energy and Environment Oriented Numerical Modeling*; InTech: Oakville, ON, Canada, 2013. [CrossRef] [PubMed]
54. Alvarado, C.; Farris, K.; Kilduff, J. Membrane Fouling, Modelling and Recent Developments for Mitigation. In *Emerging Membrane Technology for Sustainable Water Treatment*; Elsevier: Amsterdam, The Netherlands, 2016; pp. 433–462. [CrossRef]
55. Vinardell, S.; Sanchez, L.; Astals, S.; Mata-Alvarez, J.; Dosta, J.; Heran, M.; Lesage, G. Impact of permeate flux and gas sparging rate on membrane performance and process economics of granular anaerobic membrane bioreactors. *Sci. Total Environ.* **2022**, *825*, 153907. [CrossRef] [PubMed]
56. Park, J.; Kim, S.; Noh, J.; Bae, Y.; Lee, J.; Maeng, S. A shift from chemical oxygen demand to total organic carbon for stringent industrial wastewater regulations: Utilization of organic matter characteristics. *J. Environ. Manag.* **2022**, *305*, 114412. [CrossRef] [PubMed]